FeedForward Super-Twisting Sliding Mode Control for Robotic Manipulators: Application to PKMs

Hussein Saied, Ahmed Chemori, Mohamed Bouri, Maher El Rafei, Clovis Francis

FeedForward Super-Twisting Sliding Mode Control for Robotic Manipulators: Application to PKMs

Hussein Saied, Ahmed Chemori, *Senior Member, IEEE,* Mohamed Bouri, *Member, IEEE,* Maher El Rafei, *Member, IEEE,* and Clovis Francis

***Abstract*—This paper deals with the development and implementation of a novel feedforward super-twisting sliding mode controller for robotic manipulators. A full stability analysis based on a Lyapunov candidate is established showing a local asymptotic finite-time convergence of the proposed controller in the presence of upper bounded disturbances. Its robustness towards parametric uncertainties and system disturbances, thanks to the super-twisting approach, is pointed out. In addition, the feedforward dynamic term of the proposed controller that can compensate for the model nonlinearities is not sensitive to measurement noise. Real-time experiments have been conducted on two parallel manipulators: a 5-DOF SPIDER4 PKM and a 3-DOF Delta PKM. The effectiveness of the proposed controller is validated in different scenarios, including the nominal case and robustness towards parametric variations (payload) and speed changes.**

***Index Terms*—Feedforward dynamics, Sliding mode control, super-twisting SMC, parallel robots, robotic manipulators.**

I. Introduction

SLIDING Mode Control (SMC) is proposed as a robust tool against model uncertainties and time-varying parameters [1]. SMC can force the state variables of the system to converge to zero and to remain on it in the presence of system disturbances. The control law is designed based on a sliding surface feature and a discontinuous sign function which compensates the effects of the bounded disturbances. The sign function acts on switching between positive and negative feedback, which means that the system is switching between non-asymptotically stable structure and asymptotically unstable one. Using the sign function within the appropriate control law, a perfect asymptotically stable system can be gained. Therefore, the process of switching continues until we obtain asymptotic convergence of the system [2].

However, this switching produces a discontinuous control signal which is not adequate with real-time implementation. Several solutions were proposed in the literature to produce a smooth/continuous control signal and reduce the chattering, such that Quasi-Sliding Mode and Asymptotic Sliding Mode [3], [4], [5]. However, the price to be paid for obtaining a smooth control signal can be less robustness and accuracy (Quasi-Sliding Mode) or asymptotic convergence of both sliding surface and state variables (Asymptotic Sliding Mode).

Furthermore, second-order SMC algorithms can achieve finite-time convergence of the sliding variable and its derivative (Twisting and Terminal controllers) [6], [7], [8]. Moreover, the sliding dynamics are reduced to the order $(r-2)$ for the systems with relative degree r. Nevertheless, for the systems of relative degree two, the controller still produces a discontinuous control signal and chattering phenomenon persists.

Moreover, the second-order Super-Twisting SMC (ST-SMC) algorithm has been proposed and developed, resulting in an exact finite-time convergence of the sliding variable and its derivative, a high accurate asymptotic convergence of the variable states, and a continuous control signal [9].

An application of the ST-SMC algorithm to motion control systems was illustrated by numerical simulations to an under-actuated robotic system in [10] ensuring the facilitation of the motion control design and elimination of the chattering phenomenon at the outputs. In [11], the ST-SMC technique has been designed and implemented for the attitude tracking problem of a quadrotor. The implemented control law has the general formula of a computed torque approach based on the super-twisting algorithm which is able to ensure robustness with respect to bounded external disturbances. The experimental results show the good performance of the proposed controller in terms of stabilization and tracking accuracy. Another version of the model-based ST-SMC algorithm has been implemented to a mobile robot in [12] based on a continuous sliding surface (integrated error). Simulation and experimental results show better performances of the proposed controller in terms of eliminating the chattering and reducing the tracking errors compared to conventional SMCs.

Furthermore, several variable-gain ST-SMC versions have been proposed for different experimental prototypes (robotic arm [13], mass-spring-damper [14], seesaw module [15] and space robot [16]) allowing to compensate for a larger class of perturbations (by estimating the maximum bound of the perturbations) than the conventional ST-SMC and to further reduce the chattering effect of the classical first-order SMCs.

Parallel Kinematic Manipulators (PKMs) are known by their high nonlinearities which may increase considerably when operating at high-speed motions [17], [18], [19], coupled actuation, abundant uncertainties, and actuation redundancy existing in some prototypes [20]. Due to the aforementioned

Manuscript received ....

This work is supported by the French government research program, Investissements davenir through the Robotex Equipment of Excellence (ANR-10-EQPX-44).

H. Saied (e-mail: hussein.saied@lirmm.fr) and A. Chemori (email: ahmed.chemori@lirmm.fr) are with LIRMM, University of Montpellier, CNRS, Montpellier, France.

M. Bouri is with EPFL, Station 9, Lausanne CH-1015, Switzerland (email: mohamed.bouri@epfl.ch).

H. Saied, M. El Rafei (e-mail: maher.elrafei@ul.edu.lb) and C. Francis (e-mail: cfrancis@ul.edu.lb) are with CRSI, Faculty of Engineering, Lebanese University, Beirut, Lebanon.

factors, control of PKMs is considered as a very challenging task [21]. Several control solutions have been proposed in the literature for PKMs. The proposed controllers can mainly be classified into two classes: non-model-based schemes [22], [23], [24] and model-based schemes [25], [26], [19], [27], [28], [29]. Model-based controllers can provide much higher performances and robustness towards operating condition changes compared to non-model-based controllers.

Decentralized SMC has been applied to parallel manipulators such that none of the dynamic parts of the manipulator appear in the control equation. In [30], a fuzzy SMC approach is implemented on a six-degree-of-freedom (6-DOF) parallel robot showing reduced tracking error during fast motions compared to PI control. However, it is hard to guarantee the stability conditions in such a fuzzy-based controller since the control input is specified by fuzzy rules. In [31], a continuous modified twisting controller is designed for the position control of a Stewart platform. The relevance of the proposed controller has been proved by numerical simulation, showing the accurate positioning despite the presence of matched disturbances.

In [29], a SMC approach has been proposed based on the full knowledge of the 6-DOF Stewart platform dynamics given that the overall system parameters are subject to uncertainties. The stability analysis, based on the Lyapunov theory, confirmed the finite-time convergence of the sliding surface to the origin, and the experimental results proved the effectiveness of the proposed control design.

Besides, a cascaded-control algorithm based on SMC being in the outer loop was proposed in [32] for trajectory tracking control of a hydraulically driven 6-DOF parallel manipulator. Satisfactory position tracking behavior of the proposed controller has been shown through real-time experiments, compared to a proportional controller with feedforward compensation. An enhanced SMC was proposed in [33] for the real-time control of a 6-DOF Stewart platform. The augmented proposed sliding surface and the added perturbation estimator compensates effectively for the nonlinear dynamics which was considered partially unknown. The sign function was treated with a continuous approximation to avoid the resulting chattering from the hard switching. Experimental results confirmed that the proposed SMC allows to design a simple high-performance tracking control system for the Stewart platform under high payloads and large disturbance conditions. The same controller was implemented on another 2-DOF parallel manipulator, confirming again its effectiveness and good performance [34].

Another robust SMC approach with an active disturbance compensation was proposed in [35] for the trajectory tracking control of a 3-DOF vertical planar PKM, in the presence of parametric uncertainties. The considered disturbance vector compromises dynamic parameter variations, frictional effects, and other unmodelled phenomena. The efficiency and robustness of the proposed controller were proven by numerical simulations and real-time experiments in the presence of the aforementioned disturbances.

In the previous SMC-based controllers, the dynamics of the PKM was partially or fully included within the closed-loop control, assuming that the system parameters are known and subject to uncertainties. Some of the previous controllers compensate for those accommodated uncertainties by designing disturbance observers. In [36], the uncertainties resulting from parametric variations were treated by an adaptive dynamic term that updates the values of the parameters depending on the operating conditions. Real-time experiments show that the proposed adaptive terminal SMC outperforms the standard terminal SMC in terms of precision and robustness towards parametric variations (such as a handled payload).

Besides, a fuzzy SMC algorithm has been proposed for the trajectory tracking problem of a 4-DOF parallel robot in [37]. The fuzzy inference system was proposed to replace the constant switching control gain avoiding the hard chattering resulting from this term. Numerical simulations demonstrated a great reduction in the chattering with good tracking performance and robustness towards parametric uncertainties and external disturbances. Also in [38], a fuzzy SMC approach was designed based on a fuzzy neural network control theory. Numerical simulation results demonstrated the effectiveness of the proposed control method. In [39], experimental results of the implementation of a computed-torque ST-SMC on a parallel robot have been shown. The conventional computed-torque ST-SMC has shown bad behavior with high-chattering effects and mechanical vibrations. Moreover, it has been validated also through real-time experiments that a ProportionalIntegralDerivative (PID) control with feedforward dynamics can achieve better tracking performances than the conventional ST-SMC.

In this paper, a model-based feedforward ST-SMC algorithm is proposed as a control solution for robotic manipulators and validated on two PKM prototypes, SPIDER4 and Delta parallel robots. The proposed controller inherits the advantages of the ST-SMC algorithm and compensates for the nonlinear dynamics of PKMs thanks to the feedforward dynamic term. The main contributions of this paper can be summarized as follows:

1) a novel model-based formulation of ST-SMC algorithm is proposed for robotic manipulators,
2) the stability analysis of the proposed controller is established using a Lyapunov function candidate showing a finite-time convergence of the sliding variable and a local asymptotic convergence of the tracking error, and
3) experimental application to different PKM prototypes validates the efficiency of the proposed controller in terms of precision and robustness towards operating condition changes.

The rest of the paper is organized as follows. Section II introduces a background on the conventional ST-SMC algorithm for robotic manipulators. The proposed control solution is addressed in section III, with the corresponding full stability analysis. Section IV provides the description and modeling of our PKM prototypes. The issue of actuation redundancy in PKMs is addressed in section V. The obtained real-time experimental results are presented and discussed in section VI. Section VII presents some conclusions and possible future perspectives of this work.

II. Background on conventional super-twisting SMC for robotic manipulators

A. Main concept of sliding mode control

Consider the Single-Input-Single-Output (SISO) second order nonlinear uncertain system:

$$\ddot{x}_1 = f(x_1, \dot{x}_1, t) + g(x_1, \dot{x}_1, t)\nu \tag{1}$$

where $x_1, \dot{x}_1$ are the system states with x_1 being the output, ν is the scalar control signal, $f(.)$ represents the unknown bounded uncertainties and perturbations, such that $|f(.)| \leq L$ with L being a positive constant, and $g(.) \neq 0$ is the known nonlinearity. Assuming that $g(.)$ is positive and invertible for all t, the state-space presentation of (1) can be written as follows:

$$\begin{cases} \dot{x}_1 = x_2 \\ \dot{x}_2 = u + f(x,t) \end{cases} \tag{2}$$

where $x = [x_1, x_2]^T$ is the state vector and u is the control input, such that $\nu = g^{-1}(x,t)u$.

The SMC objective is to design a control signal $u(x_1, x_2)$ that drives the state variables to zero as time goes to infinity in the presence of uncertainties and perturbations $f(x,t)$ [1]. It is all about inserting a nonlinear discontinuous term into the controller responsible for rejecting the disturbances, driving the state variables to a sliding surface in a finite time, and keeping them on the surface thereafter in the presence of the bounded disturbances. A new variable in the state space representing the sliding surface is defined as follows:

$$s = x_2 + cx_1 \tag{3}$$

where c is a positive constant. The above sliding surface results with the desired compensated dynamics, $\dot{x}_1 + cx_1 = 0$, that can lead to the asymptotic convergence of $x_1, x_2 \to 0$ without any effect of the disturbance function $f(x,t)$. Applying some Lyapunov function techniques ($V = \frac{1}{2}s^2$) to the sliding surface dynamics, the required first-order SMC signal and the finite time of the reaching phase can be derived respectively as follows [1]:

$$u = -cx_2 - \rho\,\mathrm{sign}(s) \tag{4}$$

$$t_r \leq \frac{2V^{1/2}(s_0)}{\alpha} \tag{5}$$

where t_r denotes the time of reaching phase, s_0 is the sliding variable value at time $t = 0$, $\rho = L + \frac{\alpha}{\sqrt{2}}$ is the control gain, and α is a positive constant related to the reaching time.

The high-frequency switching of the introduced signum function leads to a switching control signal, zigzag behavior, due to the discrete-time nature of the control implementation. This phenomenon, known as chattering, is undesirable for practical implementations since it can harm the actuators, the mechanical parts, and the control accuracy.

The second-order super-twisting SMC algorithm can solve this issue of chattering by producing a continuous control signal. Moreover, it has an exact finite-time convergence of the sliding variable and its derivative, as well as a high accurate asymptotic convergence of the state variables.

B. Super-twisting sliding mode control

The super-twisting SMC algorithm is given as follows [9]:

$$\begin{cases} u = -k_1|s|^{\frac{1}{2}}\mathrm{sign}(s) + w \\ \dot{w} = -k_2\mathrm{sign}(s) \end{cases} \tag{6}$$

where k_1, k_2 are positive control gains. The time derivative of the sliding surface yields:

$$\dot{s} = -k_1|s|^{\frac{1}{2}}\mathrm{sign}(s) + w + f(x,t) + cx_2 \tag{7}$$

The Lyapunov candidate that proves the asymptotic stability is given as follows [40]:

$$V = \frac{1}{2}\xi^T P \xi \tag{8}$$

where $\xi = [|s|^{\frac{1}{2}}\mathrm{sign}(s) \quad w]^T$ and

$$P = \begin{pmatrix} 4k_2 + k_1^2 & -k_1 \\ -k_1 & 2 \end{pmatrix}$$

is chosen to be a positive definite matrix.

Following a similar manner as in [40], the expression of the time derivative of the Lyapunov function leads to:

$$\dot{V} = -\frac{1}{2|s|^{1/2}}\xi^T Q \xi + \frac{f(x,t)}{|s|^{1/2}}F^T\xi \tag{9}$$

where $F = [2k_2 + \frac{k_1^2}{2} \quad -\frac{k_1}{2}]^T$ and

$$Q = k_1\begin{pmatrix} 2k_2 + k_1^2 & -k_1 \\ -k_1 & 1 \end{pmatrix}$$

Knowing that the bounded perturbation satisfies $f(x,t) \leq \epsilon|s|^{1/2}$, with ϵ being a positive constant, it can be shown that

$$\dot{V} \leq -\frac{1}{|s|^{1/2}}\xi^T \tilde{Q} \xi \tag{10}$$

where

$$\tilde{Q} = \frac{k_1}{2}\begin{pmatrix} 2k_2 + k_1^2 - (\frac{4k_2}{k_1} + k_1)\epsilon & -k_1 + 2\epsilon \\ -k_1 + 2\epsilon & 1 \end{pmatrix}$$

The global asymptotic stability is achieved when $\dot{V}$ is negative definite, which means $\tilde{Q} > 0$. Thus, the control feedback gains should satisfy the following conditions:

$$\begin{aligned} k_1 &> 2\epsilon \\ k_2 &> k_1\frac{5\epsilon k_1 + 4\epsilon^2}{2(k_1 - 2\epsilon)} \end{aligned} \tag{11}$$

Furthermore, it can be shown that the states converge to zero in finite-time t_r as in (5) with $\alpha = \frac{\lambda_{min}^{1/2}\{P\}\lambda_{min}^{1/2}\{\tilde{Q}\}}{\lambda_{max}\{P\}}$, such that $\lambda_{min}\{(.)\}, \lambda_{max}\{(.)\}$ are the minimum and maximum eigen values of the matrix $(.)$ respectively.

C. Conventional super-twisting SMC for robotic manipulators

The inverse dynamic formulation of robotic manipulators can be expressed in joint space as follows [41]:

$$M(q)\ddot{q} + C(q,\dot{q})\dot{q} + G(q) + \Gamma_d = \Gamma \tag{12}$$

where $M(q)$ is the total mass and inertia matrix of the robot, $C(q,\dot{q})$ is the Coriolis and centrifugal forces matrix, $G(q)$ is the gravitational forces vector, Γ_d represents the vector of the external disturbances, uncertainties, and non-modeled phenomena, and Γ is the control input vector.

Assuming that Γ_d is bounded, the conventional ST-SMC algorithm can be designed for robotic manipulators as follows [42]:

$$\Gamma = M(q)(\ddot{r} + \Gamma_{ST-SMC}) \tag{13}$$

where $\ddot{r} = \ddot{q}_d - \lambda\dot{e}$, with λ being a positive control gain such that the tracking error is defined as $e = q - q_d$, Γ_{ST-SMC} is the control law given in (6), and $s = \dot{e} + \lambda e$ being the sliding surface. One of the main drawbacks of this control structure is the lack of dynamic compensation (it includes only the inertia matrix), which may decrease the dynamic performance of a robotic manipulator.

The control design of the ST-SMC approach, taking into account the nonlinear dynamics within a computed torque formulation, can be expressed as follows [11], [13]:

$$\Gamma = M(q)(\ddot{r} + \Gamma_{ST-SMC}) + C(q,\dot{q})\dot{q} + G(q) \tag{14}$$

The above computed torque control, based on the ST-SMC algorithm, needs an exact dynamic model to obtain good tracking performances. It relies totally on the measured joint positions and estimated joint velocities and accelerations. This can make it more sensitive to measurements noise, since the dynamic model is computed using the measured and estimated signals. Moreover, the computed-torque ST-SMC algorithm computes the dynamic term in an online mode using the measured and estimated trajectories. Obviously, the computed-torque ST-SMC algorithm can be computationally heavy, especially that the dynamic model of PKMs is known with its high nonlinearity and complexity. Thus, with computationally heavy dynamic models, this controller may face significant limitations in real-time implementations.

III. Proposed feedforward super-twisting SMC for robotic manipulators

To avoid all the above mentioned issues of conventional super-twisting algorithm, we propose to replace the computed-torque-based form with a feedforward super-twisting sliding mode control. The proposed controller takes the advantages of the standard ST-SMC algorithm, such as robustness towards disturbances, accurate convergence in the presence of external disturbances, and continuous control input. It also inherits the advantages of the feedforward dynamic term such as compensating for the structured nonlinearities, insensitivity towards measurement noise, and computation-efficiency.

A. Control design

This section provides a step-by-step derivation of the proposed feedforward ST-SMC algorithm. The standard sliding surface of a super-twisting SMC algorithm can be given as follows:

$$s = \dot{e} + \Lambda e \tag{15}$$

with $e = q_d - q$ being the tracking error, and Λ being a positive definite diagonal matrix of the control feedback gains.

Combining the defined sliding surface (15) and the dynamic system (12) leads to the following equation:

$$M(q)\big(\ddot{q}_d - \dot{s} + \Lambda\dot{e}\big) + C(q,\dot{q})\dot{q} + G(q) + \Gamma_d = \Gamma \tag{16}$$

Let us now define an auxiliary reference velocity trajectory $\dot{r} = \dot{q}_d + \Lambda e$, shifted from the actual desired one by $\Lambda\dot{e}$. Then, (16) can be rewritten as follows:

$$M(q)\ddot{r} - M(q)\dot{s} + C(q,\dot{q})\dot{q} + G(q) + \Gamma_d = \Gamma \tag{17}$$

where $\ddot{r}$ is the corresponding shifted desired acceleration. The sliding surface dynamics can be obtained from (17) as follows:

$$\dot{s} = M^{-1}(q)\Big(-\Gamma + M(q)\ddot{r} + C(q,\dot{q})\dot{q} + G(q) + \Gamma_d\Big) \tag{18}$$

Thus, the control input Γ can be chosen in a way having an exact compensation for the nonlinearities of the dynamic model, as well as theoretical compensation for the disturbance term. The conventional model-based super-twisting SMC control is defined as follows:

$$\begin{aligned}\Gamma &= M(q)\Big(\ddot{r} + K_2|s|^{\frac{1}{2}}\mathrm{sign}(s) + w\Big) + C(q,\dot{q})\dot{q} + G(q)\\ \dot{w} &= K_3\mathrm{sign}(s)\end{aligned} \tag{19}$$

where K_2, K_3 are two positive definite diagonal matrices. Note that the control law in (19) is in the form of computed torque control, based on the super-twisting algorithm.

The proposed feedforward ST-SMC algorithm comprises three main parts: (i) the feedforward term, (ii) the super-twisting algorithm, and (iii) a feedback term added to insure the stability of the system. The resulting control equation of the proposed control law is given as follows:

$$\begin{aligned}\Gamma &= M(q_d)\ddot{q}_d + C(q_d,\dot{q}_d)\dot{q}_d + G(q_d)\\ &\quad + K_1 s + K_2|s|^{\frac{1}{2}}\mathrm{sign}(s) + w\\ \dot{w} &= K_3\mathrm{sign}(s)\end{aligned} \tag{20}$$

where K_1 is a positive definite diagonal matrix of the control feedback gains.

B. Stability analysis

In order to establish the stability analysis of the proposed controller, some preliminaries should be introduced. Equation (12) inherits some properties for its dynamic terms that are useful in designing the control schemes. Some of these properties can be summarized as follows [43], [44]:

Property 1. *The mass and inertia matrix and its inverse are symmetric, positive definite, and bounded above and below as follows:*

$$m_1 \leq ||M(q)|| \leq m_2 \tag{21}$$

where $||.||$ is the second norm of a matrix, m_1 and m_2 are two positive constants.

Property 2. *The Coriolis and centrifugal matrix is bounded as follows:*

$$||C(q,\dot{q})|| \leq K_{C_1}||\dot{q}|| \tag{22}$$

where K_{C_1} is a positive constant and $||.||$ the second norm of a vector or a matrix.

Now, the stability analysis is addressed in the following theorem.

Theorem 1. *Assuming that the desired velocity is upper bounded, the joint position and velocity tracking errors ($e = q_d - q$, $\dot{e}$) of a robotic manipulator of dynamic model (12), with bounded disturbances, follow a local asymptotic convergence under the feedforward super-twisting sliding mode control given by (20), with the proper choice of Λ, K_1, K_2 and K_3 such that $det(\tilde{Q}) > 0$ and*

$$k_{h_2} \leq \Lambda \leq \frac{1 - k_C|\dot{q}_d|_M - k_{h_1}}{k_M}$$

Moreover, the local asymptotic stability is achieved in a finite time of a maximum value $T = \frac{2V^{\frac{1}{2}}(s_0)}{\gamma}$, where $s_0 = \dot{e}_0 + \Lambda e_0$ is the initial value of the sliding variable, γ is a positive constant depending on the control feedback gains Λ, K_1, K_2, K_3 and the disturbance's upper bound, and $V(s)$ is a positive radially unbounded function given in (25).

Proof. Considering the nonlinear dynamic system (12) of bounded disturbances Γ_d, the sliding variable (15), and the control equation of the proposed feedforward ST-SMC (20), one can establish the sliding variable dynamics as follows:

$$\begin{aligned} M\dot{s} = &- K_1 s - K_2|s|^{\frac{1}{2}}\text{sign}(s) - w - h(q,\dot{q}) \\ &- C\dot{e} + \Lambda M\dot{e} + \Gamma_d \end{aligned} \tag{23}$$

with $h(q,\dot{q})$ being the residual dynamics, expressed as follows:

$$\begin{aligned} h \equiv h(q,\dot{q}) = &\Big[M(q_d) - M(q)\Big]\ddot{q}_d \\ &+ \Big[C(q_d,\dot{q}_d) - C(q,\dot{q})\Big]\dot{q}_d \\ &+ \Big[G(q_d) - G(q)\Big] \end{aligned} \tag{24}$$

Without loss of generality, the scalar notation will be considered in the coming part of the stability analysis for simplicity purposes. In order to prove the stability of the dynamic system (23), consider the following Lyapunov function candidate:

$$V(s) = \frac{1}{2}\xi^T P \xi \tag{25}$$

with $\xi = [|s|^{\frac{1}{2}}\text{sign}(s), w]^T$ and

$$P = \begin{pmatrix} 4K_3 + K_2^2 & K_2 \\ K_2 & 2 \end{pmatrix} \tag{26}$$

is chosen to be a positive definite matrix. One can notice that $V(s)$ is continuously differentiable everywhere, except on $s = 0$. However, from (23), the state trajectories of the system just cross $s = 0$ and cannot stay on it, except when the origin ($s = 0$) has been reached. Thus, $V(s)$ is differentiable for almost every t and one can apply Lyapunov's theorem for the points where $V(s)$ is differentiable [40].

The solutions of the discontinuous differential equation (23) are interpreted as the ones of the differential inclusion $\dot{s} \in f(s)$. The signum function $\text{sign}(s)$ belongs to the interval $[-1, 1]$ for $s = 0$. Then, since $0 \in f(0) = [-1, 1]$, it follows that $s = 0$ is an equilibrium point [40]. The time derivative of $V(s)$ along the solutions of the system leads to the following:

$$\dot{V} = -\frac{1}{2M|s|^{\frac{1}{2}}}\xi^T Q \xi + \frac{1}{2M|s|^{\frac{1}{2}}} f(s,t) F^T \xi \tag{27}$$

where $F = [K_2^2 + 4K_3, \quad K_2]^T$, $f(s,t) = \Big(\Gamma_d - K_1 s - (C - \Lambda M)\dot{e} - h\Big)$, and

$$Q = \begin{pmatrix} K_2^3 + 4K_2K_3 + 2K_2K_3M & K_2^2 + 2K_3 - 2K_3M \\ K_2^2 + 2K_3 - 2K_3M & K_2 \end{pmatrix} \tag{28}$$

M is positive (or positive definite matrix in non-scalar case) and K_2, K_3 are chosen such that Q is positive definite matrix. The perturbation term $|f(s,t)|$ can be upper bounded as follows:

$$|f(s,t)| \leq K_1|s| + |C|\ |\dot{e}| + \Lambda|M|\ |\dot{e}| + |h| + |\Gamma_d| \tag{29}$$

According to [44], the Euclidean norm of the residual dynamics of a robotic manipulator ($||h(q,\dot{q})||$) can be upper bounded as follows (for vector form):

$$||h(q,\dot{q})|| \leq k_{h_1}||\dot{e}|| + k_{h_2}||e|| \tag{30}$$

where k_{h_1}, k_{h_2} are two positive constants. For the scalar case, $|h| \leq k_{h_1}|\dot{e}| + k_{h_2}|e|$. By the use of Properties 1 and 2, and assuming that the disturbance function is globally bounded by $|\Gamma_d| \leq \epsilon|s|$, such that $\epsilon > 0$, the inequality (29) can be developed as follows:

$$\begin{aligned} |f(s,t)| \leq &\big(K_1 + \epsilon\big)|s| \\ &+ \big(k_C|\dot{q}_d|_M + \Lambda k_M + k_{h_1}\big)|\dot{e}| \\ &+ k_{h_2}|e| + k_C|\dot{e}|^2 \end{aligned} \tag{31}$$

where k_C, k_M are two positive constants, $|\dot{q}_d|_M$ is the upper bound of the the desired velocity trajectory. For small values of ($|\dot{e}|$) (when s is around the origin), the linear term $\big(k_C|\dot{q}_d|_M + \Lambda k_M + k_{h_1}\big)|\dot{e}|$ dominates the quadratic term $k_C|\dot{e}|^2$. Then, assuming that $\big(k_C|\dot{q}_d|_M + \Lambda k_M + k_{h_1}\big) \leq 1$ and $k_{h_2} \leq \Lambda$, the term $|f(s,t)|$ can be locally upper bounded as follows:

$$|f(s,t)| \leq \mu\ |s| \tag{32}$$

with $\mu = K_1 + \epsilon + 1$. Moreover, if s is around the origin, it implies that $|s| \leq |s|^{\frac{1}{2}}$. Thus, (32) can be expressed as follows:

$$|f(s,t)| \leq \mu \ |s|^{\frac{1}{2}} \tag{33}$$

Making use of (33), $\dot{V}(s)$ in (27) can be locally upper bounded as follows:

$$\dot{V} \leq -\frac{1}{2M|s|^{\frac{1}{2}}}\xi^T Q \xi + \frac{\mu}{2M|s|^{\frac{1}{2}}}|s|^{\frac{1}{2}} \ |F^T \xi| \tag{34}$$

Then, (34) can be reformulated as follows:

$$\dot{V} \leq -\frac{1}{2M|s|^{\frac{1}{2}}}\xi^T Q \xi + \frac{1}{2M|s|^{\frac{1}{2}}}\xi^T Q_1 \xi \tag{35}$$

with

$$Q_1 = \mu \begin{pmatrix} K_2^2 + 4K_3 & \frac{1}{2}K_2 \\ \frac{1}{2}K_2 & 0 \end{pmatrix}$$

leading to

$$\begin{aligned} \dot{V} &\leq -\frac{1}{2M|s|^{\frac{1}{2}}}\xi^T \tilde{Q} \xi \\ \dot{V} &\leq -\frac{1}{2M|s|^{\frac{1}{2}}}\lambda_{min}\{\tilde{Q}\} \ ||\xi||^2 \end{aligned} \tag{36}$$

where

$$\tilde{Q} = \begin{pmatrix} K_2^3 + 4K_2K_3 + 2K_2K_3M - \mu(K_2^2 + 4K_3) & \\ K_2^2 + 2K_3 - 2K_3M - \frac{\mu}{2}K_2 & \\ & K_2^2 + 2K_3 - 2K_3M - \frac{\mu}{2}K_2 \\ & K_2 \end{pmatrix} \tag{37}$$

with $\lambda_{min}\{\tilde{Q}\}$ is the minimum eigen value of $\tilde{Q}$ and $||\xi||$ is the Euclidean norm of vector ξ. $\dot{V}$ is negative definite if $\tilde{Q}$ is a positive definite matrix. Then, following Lyapunov's direct method, if Λ, K_1, K_2, K_3 are selected such that $det(\tilde{Q}) > 0$ and $k_{h_2} \leq \Lambda \leq \frac{1-k_C|\dot{q}_d|_M - k_{h_1}}{k_M}$, the origin $s = 0$ is an equilibrium point that is locally asymptotically stable.

Furthermore, $V(s)$ is positive definite and radially unbounded by the following [40]:

$$\frac{1}{2}\lambda_{min}\{P\} \ ||\xi||^2 \leq V(s) \leq \frac{1}{2}\lambda_{max}\{P\} \ ||\xi||^2 \tag{38}$$

where $||\xi||^2 = |s| + w^2$ is the square of the Euclidean norm of ξ, $\lambda_{min}\{A\}$ and $\lambda_{max}\{A\}$ are the minimum and maximum eigen values respectively of any matrix A. Making use of (38), (36), and the fact that

$$|s|^{\frac{1}{2}} \leq ||\xi|| \leq \frac{\sqrt{2} \ V^{\frac{1}{2}}}{\lambda_{min}^{1/2}\{P\}}, \tag{39}$$

it can be shown that $\dot{V}$ is upper bounded as follows:

$$\dot{V} \leq -\gamma V^{\frac{1}{2}} \tag{40}$$

where

$$\gamma = \frac{\lambda_{min}^{1/2}\{P\} \ \ \lambda_{min}\{\tilde{Q}\}}{\sqrt{2}M \ \ \lambda_{max}\{P\}} \tag{41}$$

The differential equation $\dot{\nu}(t) = -\gamma \nu^{1/2}(t)$ for $\nu(0) = \nu_0 \geq 0$ has a solution expressed by: $\nu(t) = \left(\nu_0^{\frac{1}{2}} - \frac{\gamma}{2}t\right)^2$. Then, following the comparison principle [45] that says $V(t) \leq \nu(t)$ when $V(s_0) \leq \nu_0$, one can conclude that $V(s(t))$, and therefore $s(t)$, converges to zero in finite time at most after $T = \frac{2V^{\frac{1}{2}}(s_0)}{\gamma}$, and the proof is concluded. □

IV. Description and Modeling of PKM Prototypes

A. SPIDER4 robot: a 5-DOF redundant PKM

SPIDER4 robot is a Delta-like redundantly actuated parallel manipulator designed and fabricated at LIRMM with the cooperation of TECNALIA, a research and innovation organisation located in Spain. The intention behind this platform is to perform machining operations with high dynamic performance, high precision, and dexterity.

SPIDER4 PKM structure consists of a fixed-base holding four high-torque actuators, each linked to a rear-arm through a revolute joint (cf. Fig. 1). The reference frame $\{O_b, x_b, y_b, z_b\}$, attached to the fixed-base, is illustrated in Fig. 1. Two parallel rods forming a forearm are connected to each rear-arm, as well as to the traveling-plate by means of universal joints. The traveling-plate (also referred to as the nacelle) is allowed to move along three translational axes x, y and z. Additional independent serial wrist mechanism (actuated with two motors) is attached to the nacelle, offering two more rotational movements for the machining spindle around the axes of the motors M_1 and M_2 as illustrated in Fig. 1. Thus, SPIDER4 robot is a 5-DOF redundant parallel manipulator with one degree of actuation redundancy. It is worth to mention that the overall dimensions of SPIDER4 with the tooling are 4600 mm in length, 2500 mm in width and 2400 mm in height as illustrated in Fig. 2. In this work, we are concerned only with the parallel structure of SPIDER4 PKM proposing control solution for the trajectory tracking problem of the nacelle in the workspace. Consider $X = [x, y, z]^T$ as the Cartesian position vector of the nacelle and $q = [q_1, q_2, q_3, q_4]^T$ as the joint position vector, representing the configuration of the actuated joints. For more datails about SPIDER4 parallel robot, the reader can refer to [46] [47].

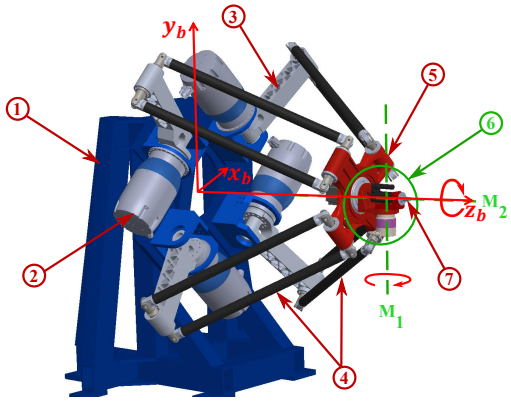

Fig. 1. A schematic view of SPIDER4 parallel robot including ①: Fixed-base, ②: Actuator, ③: Rear-arm, ④: Forearm, ⑤: Nacelle, ⑥: Serial wrist mechanism, ⑦: Spindle.

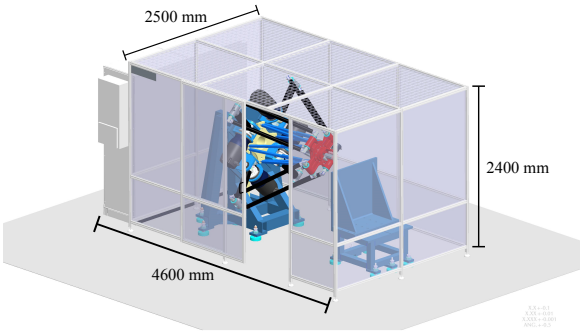

Fig. 2. SPIDER4 parallel robot overall system dimensions (in mm)

B. Delta robot: a 3-DOF non-redundant PKM

The Delta robot has been invented by prof. Reymond Clavel at Ecole Polytechnique Federale de Lausanne (EPFL), Switzerland [48]. It was mainly designed for industrial applications that need pick-and-place cycle motions. Its smart design enables it to operate at very high accelerations, thanks to the minimized mass and inertia of the mechanical parts which are supposed to be in motion. Fig. 3 shows a kinematic illustration of Delta robot and its main components. The reference frame $\{O_b, x_b, y_b, z_b\}$ is attached to the center of the fixed-base.

The overall structure is composed of three actuators integrated to a fixed-base, three kinematic chains and one moving platform (called also traveling-plate). The shaft of each motor is connected to an extremity of a rear-arm supposed to make rotation through a revolute joint. The second extremity of the rear-arm is linked to two parallel rods through ball-and-socket passive joints. The parallel rods are also linked to the traveling-plate from their other extremity through the same said joints. The synchronized control of the three arms allows the traveling-plate to move within three basic translational DOFs (x, y and z), conserving its parallelism property with respect to the fixed-base. The robot is considered as a non-redundant PKM, because the number of actuators is equal to the number of the output DOFs.

Let $X = [x, y, z]^T$ represents the Cartesian position of the traveling plate, and $q = [q_1, q_2, q_3]^T$ represents the unique and straightforward inverse kinematic solution of the joint angles.

C. Dynamics of parallel PKMs

The dynamic model of Delta-like parallel manipulators is introduced in this section, as in [49], based on the virtual work principle described in [50]. Consider the two scalars "n" and "m_{DOF}" representing the number of actuators and DOFs, respectively. As common for Delta-like PKMs, the following two assumptions are considered for simplification purposes:

Assumption 1. *Both dry and viscous frictions, in all passive and active joints, are neglected.*

Assumption 2. *The forearms' mass is split up into two point-masses, the first one is added to the mass of the rear-arms, while the second is considered with the mass of the traveling-plate (cf. illustration of Fig. 4).*

Looking for the dynamics of the traveling-plate, one can define two kinds of forces acting on it: the gravitational force $G_{tp} \in \mathbb{R}^m$ and the inertial force $F_{tp} \in \mathbb{R}^m$.

Back to Assumption 2, the total mass of the traveling-plate including the half-masses of the forearms can be calculated as follows:

$$m_{tp} = m_p + n\frac{m_f}{2} \tag{42}$$

where m_p is the own mass of the traveling-plate and m_f is the mass of each forearm, as illustrated in Fig. 4.

Then, the gravitational force acting on the traveling-plate can be expressed as follows:

$$G_{tp} = -M_{tp}G \tag{43}$$

where $M_{tp} \in \mathbb{R}^{m\times m}$ is the diagonal mass matrix of the traveling-plate, $G \in \mathbb{R}^m$ is the gravity vector (for Delta parallel robot $G = [0\ 0\ g]^T$, and for SPIDER4 parallel robot $G = [0\ g\ 0]^T$), being $g = 9.81\ m/s^2$ the gravity acceleration.

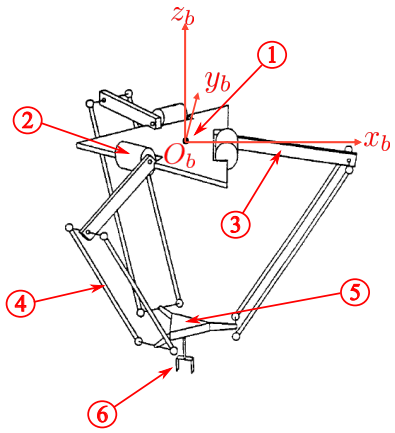

Fig. 3. A schematic view of Delta parallel robot including ①: Fixed-base, ②: Actuator, ③: Rear-arm, ④: Forearm, ⑤: Traveling-plate, ⑥: End-effector.

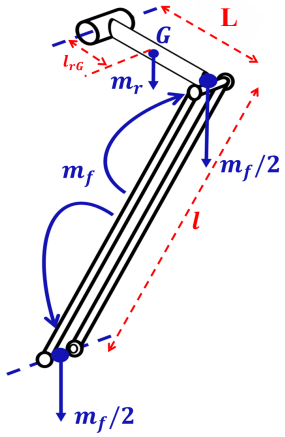

Fig. 4. Illustration of dynamic parameters of Delta parallel robot arms.

The inertial force acting on the traveling-plate arising from its acceleration is defined as follows:

$$F_{tp} = M_{tp}\ddot{X} \tag{44}$$

where $\ddot{X} \in \mathbb{R}^m$ denotes the Cartesian acceleration vector.

The contributions of the gravitational and inertial forces to the actuator torques are evaluated using the Jacobian matrix as follows:

$$\Gamma_{G_{tp}} = J^T G_{tp} \tag{45}$$

$$\Gamma_{F_{tp}} = J^T F_{tp} \tag{46}$$

Besides, the dynamics from the actuators side includes the contributions of forces acting on the rear-arms. Here, we name three contributing forces: (i) the actuators input torque $\Gamma \in \mathbb{R}^n$, (ii) the effect of the rear-arms gravitational forces $\Gamma_{G_{arm}} \in \mathbb{R}^n$, and (iii) the inertial contribution due to rear-arms acceleration $\Gamma_{arm} \in \mathbb{R}^n$.

The contribution of the rear-arms gravitational forces, taking into consideration the statement of Assumption 2, can be given as follows:

$$\Gamma_{G_{arm}} = -g\ M_r\ Cos(q) \tag{47}$$

with $Cos(q) \in \mathbb{R}^n$, $M_r \in \mathbb{R}^{n\times n}$ is a diagonal matrix that includes some dynamic parameters such as: the mass of each rear-arm m_r, the distance from the axis of rotation of each rear-arm to its center of gravity l_{r_G}, and the complete length of each rear-arm L.

The inertial contribution of the operating acceleration of the rear-arms can be defined as follows:

$$\Gamma_{arm} = I_{arm}\ddot{q} \tag{48}$$

where $I_{arm} \in \mathbb{R}^{n\times n}$ is a diagonal inertia matrix including the inertia of the actuators, the rear-arms and the half-masses of the forearms with respect to the actuators' rotation axes. The vector $\ddot{q} \in \mathbb{R}^n$ denotes the acceleration in joint space.

After applying the virtual work principle, stating that the contribution of all non-inertial forces must be equal to the contribution of all inertial forces, one can formulate the resulting inverse dynamic model as follows:

$$\Gamma = I_{arm}\ddot{q} + J^T M_{tp}\ddot{X} + \Gamma_{G_{tp}} + \Gamma_{G_{arm}} \tag{49}$$

The relation between joint and Cartesian accelerations can be expressed as follows:

$$\ddot{X} = J\ddot{q} + \dot{J}\dot{q} \tag{50}$$

where $\dot{J}$ is the time derivative of J.

Now, by substituting (50) in (49) and rearranging the terms, we obtain the inverse dynamic model of a Delta-like parallel robot in the joint space as follows:

$$\Gamma(t) = M(q)\ddot{q} + C(q,\dot{q})\dot{q} + G(q) \tag{51}$$

where $M(q) = I_{arm} + J^T M_{tp} J$ is the total mass and inertia matrix of the robot, $C(q,\dot{q}) = J^T M_{tp}\dot{J}$ is the Coriolis and centrifugal forces matrix, $G(q) = -\Gamma_{G_{tp}} - \Gamma_{G_{arm}}$ is the gravitational forces vector, and $\Gamma(t)$ is the control input vector.

The main dynamic parameters of SPIDER4 and delta parallel robots are summarized in Tables I and II, respectively. Since SPIDER4 and Delta are translational robots, the direct kinematic model have been used to quantify the range of Cartesian error and not the absolute error. Knowing that the calibration of kinematic model does not change that much the range of errors, it was not conducted. This can be explained by the fact that errors between joint and tool spaces are associated through the Jacobian matrix. The link lengths have been measured on the robots after manufacturing and adjusted accordingly in the models. All the offset error effects are canceled after the time derivative applicat.

V. The issue of actuation redundancy in PKMs

Actuation redundancy in parallel manipulators can be achieved by adding additional actuated kinematic chains. It brings several advantages to parallel manipulators such as: eliminating singularities, increasing the workspace, reducing the energy consumption, and adding more stiffness to the structure. However, it may produce some antagonistic forces that have no effect on the motion of the manipulator, and appear as internal forces called prestress [51].

These internal forces are caused by the generated control forces that fall in the null space of the inverse Jacobian matrix. The generated control forces may deteriorate the global performance, especially in the presence of measurements errors. However, those forces can be eliminated by projecting the control forces vector into the range space of the inverse Jacobian matrix as follows [52]:

$$\Gamma^* = R_{J_m^T}\Gamma \tag{52}$$

where Γ^* is the effective control input forces, applied to the redundant parallel manipulator, and $R_{J_m^T} = J_m^{T^+} J_m^T$ is the projection operator, called also the regularization matrix.

In this work, for the redundantly actuated parallel manipulator (i.e. SPIDER4 robot), the generated control input from a control solution, is treated by the projection method, introduced in (52), before feeding it to the actuators.

VI. Real-time experiments and results

A. Experimental platforms and implementation issues

1) Experimental testbeds:

TABLE I
THE MAIN DYNAMIC PARAMETERS OF SPIDER4 PARALLEL ROBOT.

Parameter	Description	Value
L	Rear-arm length	535 mm
l	Forearm length	1100 mm
m_r	Rear-arm mass	17.6 kg
m_f	Forearm mass	4.64 kg
m_{tp}	Total traveling-plate mass	51.54 kg
I_{arm}	Rear-arm inertia	1.69 kg.m^2
I_{act}	Actuator inertia	2.23 $\times 10^{-3}$ kg.m^2

TABLE II
THE MAIN DYNAMIC PARAMETERS OF DELTA PARALLEL ROBOT.

Parameter	Description	Value
L	Rear-arm length	240 mm
l	Forearm length	480 mm
m_r	Rear-arm mass	0.0653 kg
m_f	Forearm mass	0.084 kg
m_p	Own traveling-plate mass	0.305 kg
I_{act}	Actuator inertia	1.82 $\times 10^{-3}$ kg.m^2

Fig. 5. View of the SPIDER4 parallel robot experimental platform.

a) Experimental testbed of the 5-DOF SPIDER4 parallel robot: The real-time experimental platform of SPIDER4 robot is shown in Fig. 5. The parallel structure of SPIDER4 robot consists of four TPM$^+$ high-torque rotary motors responsible for generating the three translational motions x, y and z at the level of the nacelle. A gearbox with a gear ratio of 22 is merged seamlessly to the motor forming one compact versatile unit.

The peak torque that can be delivered by one motor, after the gear transformation, reaches up to 3100 Nm. The maximum speed for each motor after the gear can reach up to 189 rpm. The overall structure provides at the traveling-plate level a maximum speed of $2\,m/s$ and a maximum acceleration of 4 G.

The control program of SPIDER4 robot is established within Matlab/Simulink environment from MathWorks. Using the library of B&R automation studio, a target for Simulink tool compiles the code and automatically converts it to C/C++ language, which can be accessible from Automation Studio software provided by B&R. The reference trajectory generation process is done using the numerical control programming language named G-code (Geometric Code), used mostly in CNC machines (Computer Numerical Control machines).

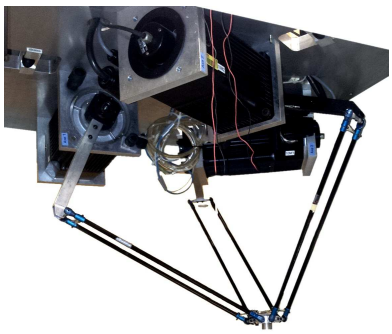

Fig. 6. View of the Delta parallel robot experimental platform.

The overall program is then downloaded to an industrial control PC (APC910) from B&R responsible of communication with the motion control system. The operational clock cycle of its processor is 2.5 KHz, leading to a sampling period of 0.4 ms. The motion control of SPIDER4 robot consists of X20 modules and inverter modules named ACOPOS multi system, the new drive generation from B&R Perfection in Automation.

b) Experimental testbed of the 3-DOF Delta parallel robot: The Delta parallel robot, used for the real-time experiments, is shown in Fig. 6. It is located at Robotic Systems Laboratory, EPFL, Switzerland. Three direct-drive motors, integrated to the fixed-base, allow the translational motion of the traveling-plate. Each motor can deliver a maximum torque of 23 Nm. The overall mechanical structure can reach up to 50 G as peak acceleration.

The control algorithms are implemented in C++ language using Visual Studio software from Microsoft, running under a Windows XP operating system. RTX extension is used to establish the real-time communication. The internal timer (HAL timer) of RTX is configured to $100\,\mu s$, in which the control loop is set to 10 times this value for synchronization, leading to a sample time of 1 ms, and a sampling frequency of 1 KHz.

2) Reference trajectory generation:

a) SPIDER4 parallel robot reference trajectory: As said before, the trajectory generation of SPIDER4 robot uses the programming language for CNC machines known as G-Code. The generated trajectory of SPIDER4 robot considered for the experimental tests employs the two types of motion: feed and circular movements. The feed movement is expressed in the G-code instructions as G1 linear interpolation. The circular movement is presented in the G-code instructions as G3 circular interpolation.

Using G1 and G3 interpolations, the G-Code generating the desired trajectory of SPIDER4 robot is written. A 3D view of the generated trajectory is sketched in Fig. 7, illustrating the points traversed by the robot within the workspace. The sequence of the interpolated points of the desired trajectory is given in the following order:

1) Linear motion: P_0, P_1.
2) Circular motion: from P_1 to P_1, following a circle of a diameter D_2.
3) Circular motion: from P_1 to P_1, following a circle of a diameter D_1.
4) Linear motion: P_1, P_0.
5) Circular motion: from P_0 to P_0, following a circle of a diameter D_3.

b) Delta parallel robot reference trajectory: The motion profile used for Delta robot is a point-to-point movement. It

means that from a stop point, the robot accelerates to reach a constant velocity. Then, the robot decelerates such that the final acceleration, and velocity, are zero at the final desired point.

The reference trajectory is generated using semi-ellipse geometric motions, producing a pick-and-place trajectory in Cartesian space. This trajectory is mainly used in industry for food packaging applications. A 3D illustrative view is shown in Fig. 8 for the pick-and-place cycle to be followed by the robot's traveling-plate.

3) Performance evaluation indices: In order to quantify the relevance of the control algorithms, we need to define a certain performance index. One of our main objectives is to enhance the precision and increase the tracking accuracy of the parallel robots through the proposed controllers.

Thus, an accuracy evaluation tool frequently used to evaluate differences between a desired trajectory and an actual one is the Root-Mean-Square Error (RMSE) criterion. It can quantify the tracking error, between the desired trajectory and the actual one.

For both PKM prototypes (i.e. SPIDER4 and Delta), the actuated joint positions are measured using encoders equipping the motors, and the actual Cartesian position vectors are then computed using the forward kinematic models.

For Cartesian space, the performance index of the translational motions is defined as $RMSE_T$. For joint space, the performance index is defined as $RMSE_J$. Then, these performance indices can be expressed as follows:

$$RMSE_T = \sqrt{\frac{1}{N}\sum_{i=1}^{N}\Big(\sum_{j=1}^{m}\big(e_x^2(i)\big)\Big)}$$
$$RMSE_J = \sqrt{\frac{1}{N}\sum_{i=1}^{N}\Big(\sum_{j=1}^{n}\big(e_j^2(i)\big)\Big)} \quad (53)$$

where N denotes the number of the collected samples overall the whole trajectory, e represents the difference between the desired and measured positions (in Cartesian (i.e. e_x) or in joint (i.e. e_j) spaces).

In order to estimate the energy consumption, an input-torques-based criterion is adopted as follows:

$$E_\Gamma = \sum_{j=1}^{n}\sum_{i=1}^{N}|\Gamma_j(i)| \quad (54)$$

where E_Γ is the total summation of the absolute values of the input torques, delivered by the n actuators.

4) Tuning of the control feedback gains: A popular method for tuning of the control feedback gains in experiments, used particularly for complex robotic systems, is the Trial-and-Error method. It is characterized by trying manually and continuously different sets of control gains in real-time framework until the desired control performance is reached. It is mostly used when the formulated dynamic model does not exactly match the physical system, and thus the automatic numerical closed-loop tuning methods may give unsuitable control gains for real-time experiments.

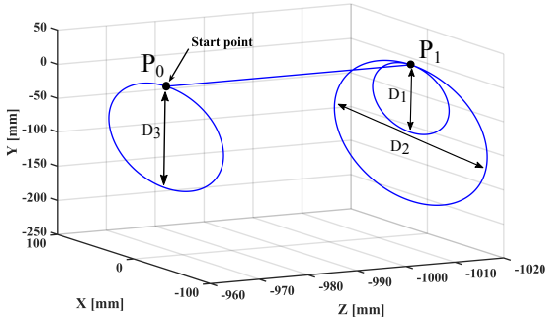

Fig. 7. 3D view of the reference trajectory of SPIDER4 parallel robot.

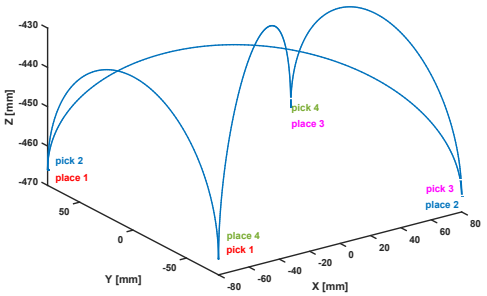

Fig. 8. 3D view of the reference trajectory of Delta parallel robot.

B. Validation on SPIDER4 parallel robot

In the sequel, the experimental results on SPIDER4 robot of a PIDFF control, the conventional Computed-Torque Super-Twisting SMC (CT-ST-SMC) algorithm, and the proposed FF-ST-SMC algorithm are demonstrated. Two main scenarios are conducted in this experimental demonstration, including nominal case, and robustness towards speed changes. The control gains of the implemented controllers are summarized in Table III.

1) Scenario 1: nominal case: This scenario allows the robot's nacelle to follow the desired trajectory with a speed of 2540 mm/s.

The Cartesian tracking errors of the conventional CT-ST-SMC and the PIDFF control are depicted in Fig. 9. It is clear that the tracking errors of a PIDFF control are smaller than those of the CT-ST-SMC along the reference trajectory. Note that increasing the control gains of CT-ST-SMC algorithm

TABLE III
THE CONTROL GAINS USED ON SPIDER4 ROBOT.

Standard PIDFF	Proposed FF-ST-SMC	Conventional CT-ST-SMC
$K_p = 3500$	$\Lambda = 90$	$\Lambda = 80$
$K_d = 40$	$K_1 = 7.5$	$K_1 = 3$
$K_i = 1500$	$K_2 = 5$	$K_2 = 2$
	$K_3 = 25$	$K_3 = 18$

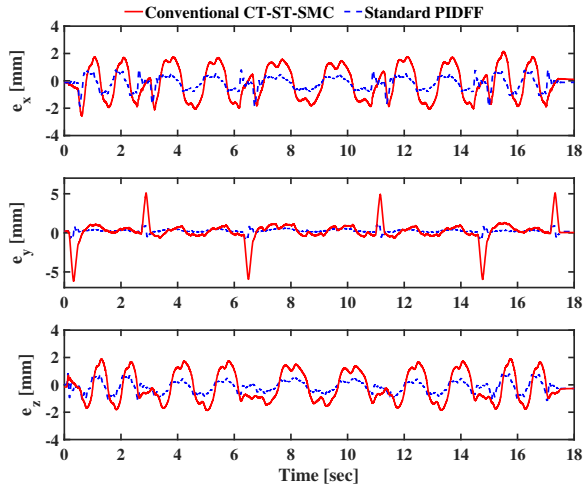

Fig. 9. Scenario 1: Evolution of Cartesian tracking errors of CT-ST-SMC and PIDFF controllers on SPIDER4 parallel robot

generated more vibrations through the mechanical system of the robot. This can be explained by the high effect of measurements noise when using the conventional CT-ST-SMC algorithm since it relies totally on the measured signals and not the desired ones. Thus, the standard PIDFF control overcomes the conventional CT-ST-SMC algorithm in terms of tracking precision.

The RMSE performance indices of the Cartesian and joint tracking errors are evaluated for CT-ST-SMC and PIDFF controllers over all the reference trajectory and the obtained values are summarized in Table IV. One can observe that a PIDFF is much better than the conventional CT-ST-SMC in terms of tracking precision.

The generated control input torques of the four motors of SPIDER4 robot, for PIDFF and CT-ST-SMC controllers, are displayed in Fig. 10. Both control algorithms generate control signals within the admissible limit of the motors. Note that the control signals of the CT-ST-SMC controller have a higher frequency than that of the standard PIDFF. This is not safe for the robot and may lead to a harmful behavior.

Following the same trajectory, the Cartesian tracking errors for the standard PIDFF and the proposed FF-ST-SMC are recorded and plotted in Fig. 11. One can observe a good error regulation is performed by the proposed controller on all the translational axes, compared to the classical PIDFF control. In particular, the tracking error along y-axis is significantly reduced by the proposed controller as shown clearly in Fig. 11. Due to the horizontal inclination of SPIDER4 robot and its heavy parts, the y-axis motion is highly subject to the effect of the gravity. Thus, we can notice from the tracking errors that the proposed FF-ST-SMC is more robust towards gravitational effects than the standard PIDFF controller.

The RMSE performance indices, of the Cartesian and joint tracking errors, are evaluated for both controllers over the whole reference trajectory and the obtained metrics are summarized in Table IV. A significant improvement in the dynamic performance, by the proposed FF-ST-SMC algorithm w.r.t the standard PIDFF, is obtained. The RMSE is reduced

TABLE IV
SCENARIO 1: CONTROL PERFORMANCE EVALUATIONS OF THE IMPLEMENTED CONTROLLERS ON SPIDER4 PARALLEL ROBOT.

	$RMSE_T$ [mm]	$RMSE_J$ [deg]
Conventional CT-ST-SMC	1.9895	0.2751
Standard PIDFF	0.6026	0.0472
Proposed FF-ST-SMC	0.2689	0.0264
Improvements on CT-ST-SMC	86.5 %	90.4 %
Improvements on PIDFF	55.4 %	44.1 %

by 55.4 % in the Cartesian space , and by 44.1 % in the joint space. Moreover, the proposed controller improves the performance w.r.t the conventional CT-ST-SMC algorithm by 86.5 % and 90.4 % in Cartesian and joint spaces respectively.

Compared to the PIDFF control structure, the FF-ST-SMC approach has two sign-based functions in terms of the sliding surface, instead of the integral term in the PIDFF. These robust functions proved experimentally their significant performance in terms of disturbance-rejection during dynamic motions and stationary positions (at the end of the trajectory, see Fig. 11).

The generated control input torques of the four motors of SPIDER4 robot, for PIDFF and proposed controllers, are illustrated in Fig. 12. It is clear that both control algorithms generate control signals within the admissible limit of the motors.

In this scenario, the superiority of the proposed FF-ST-SMC algorithm over the conventional CT-ST-SMC and PIDFF controllers has been validated. Thanks to its robustness towards measurements noise and low computational efforts, the relevance of the proposed controller was proved.

2) Scenario 2: robustness towards speed changes: In this scenario, the speed of the robot's nacelle is increased to 15240 mm/s, following the reference trajectory. The intention behind this scenario is to test the performance of the proposed controller at high-speed motions when the nonlinearity effects of parallel manipulators increase considerably. The results of the standard PIDFF and the proposed FF-ST-SMC controllers

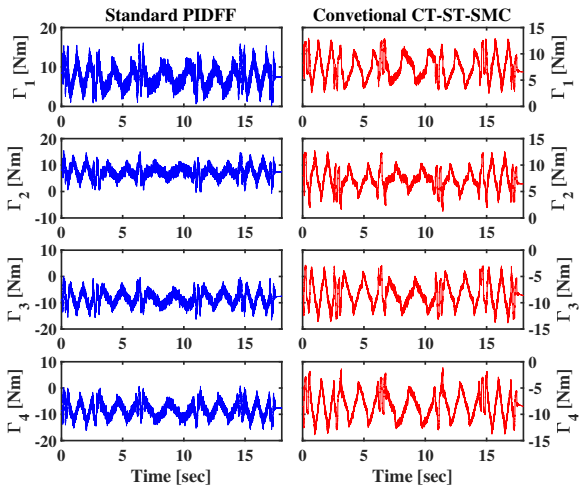

Fig. 10. Scenario 1: Evolution of input control signals generated by CT-ST-SMC and PIDFF controllers on SPIDER4 parallel robot.

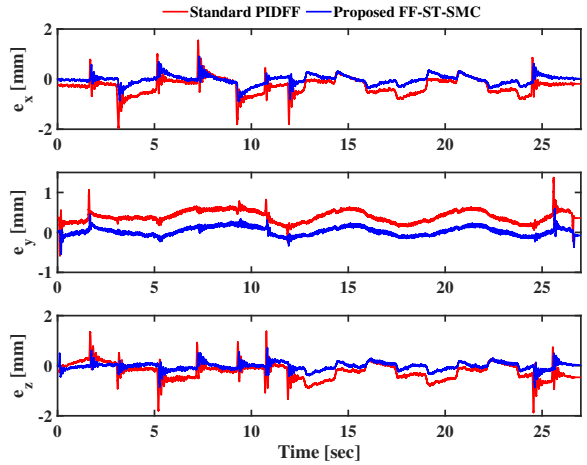

Fig. 11. Scenario 1: Evolution of the Cartesian tracking errors of PIDFF and FF-ST-SMC controllers on SPIDER4 parallel robot.

are shown in the sequel. The conventional CT-ST-SMC algorithm has produced a lot of mechanical vibrations in this scenario and it was harmful to operate the robot overall the whole trajectory.

The Cartesian tracking errors for both controllers are depicted in Fig. 13. The proposed FF-ST-SMC controller performs better than standard PIDFF in terms of precision. The dynamic error is reduced considerably by the proposed controller, compared to the PIDFF control law as well as the static error.

The evaluations of the performance indices of both controllers are summarized in Table V. Remarkable improvements are obtained by the proposed controller, compared to the standard PIDFF. The RMSE in Cartesian space is reduced by 44.3 %, while that of joint space is also reduced by 38.4 %. The disturbance-rejection and high nonlinearities compensation at high-speed motions are verified by the proposed FF-ST-SMC approach.

The evolution of the control input torques, generated by the two controllers, is plotted in Fig. 14. The control signals show

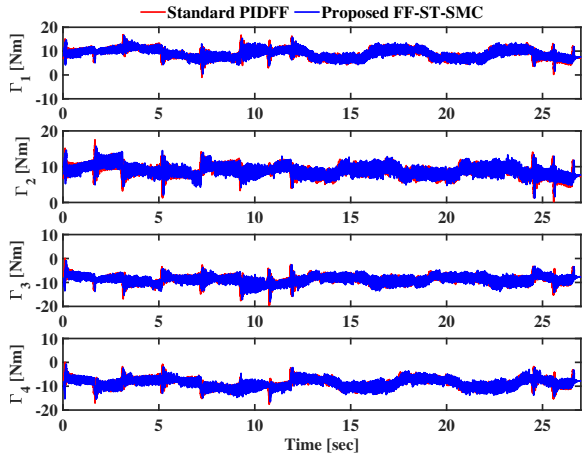

Fig. 12. Scenario 1: Evolution of the control input torques of PIDFF and FF-ST-SMC controllers on SPIDER4 parallel robot.

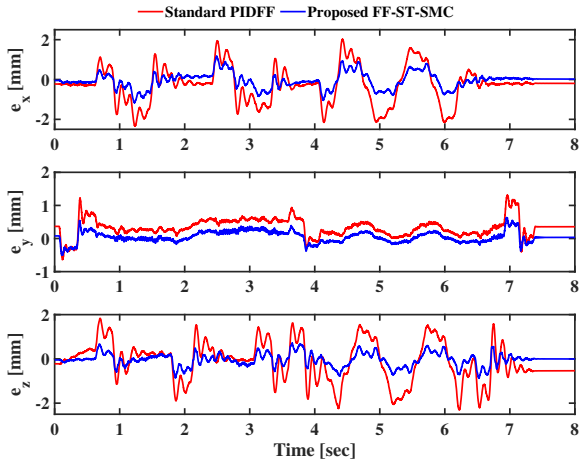

Fig. 13. Scenario 2: Evolution of the Cartesian tracking errors of both controllers on SPIDER4 parallel robot.

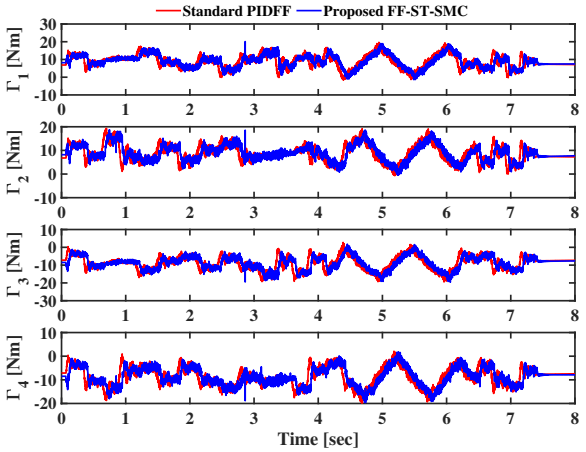

Fig. 14. Scenario 2: Evolution of the control input torques of both controllers on SPIDER4 parallel robot.

a good behavior within the admissible limit of the motors.

Last but not least, the real-time experiments on SPIDER4 robot of the proposed feedforward ST-SMC have shown a good global performance at low and high dynamic operating conditions, compared to the standard feedforward PID controller.

C. Validation on Delta parallel robot

In order to validate the proposed feedforward super-twisting SMC approach for pick-and-place industrial operations, real-time experiments of the standard PIDFF controller and the proposed one are conducted on the Delta parallel robot.

TABLE V
SCENARIO 2: CONTROL PERFORMANCE EVALUATION OF BOTH CONTROLLERS ON SPIDER4 PARALLEL ROBOT.

	$RMSE_T$ [mm]	$RMSE_J$ [deg]
Standard PIDFF	0.92064	0.08421
Proposed FF-ST-SMC	0.5127	0.0519
Improvements	44.3 %	38.4 %

TABLE VI
THE CONTROL GAINS OF BOTH CONTROLLERS USED ON DELTA PARALLEL ROBOT.

Standard PIDFF	**Proposed FF-ST-SMC**
$K_p = 720$	$\Lambda = 360$
$K_d = 2$	$K_1 = 0.25$
$K_i = 3600$	$K_2 = 1.5$
	$K_3 = 2$

TABLE VII
SCENARIO 1: CONTROL PERFORMANCE EVALUATION OF BOTH CONTROLLERS USED ON DELTA PARALLEL ROBOT.

	$RMSE_T$ [mm]	$RMSE_J$ [deg]	E_Γ [Nm]
Standard PIDFF	0.1392	0.0362	2.9486×10^4
Proposed FF-ST-SMC	0.1031	0.025	2.3737×10^4
Improvements	26 %	31%	19.5 %

In this experimental demonstration, three scenarios are adopted, including nominal case, robustness towards payload and speed changes, and robustness towards very high accelerations. The control feedback gains, obtained by Trial-and-Error tuning method on the real-time experimental platform, are summarized in Table VI.

1) Scenario 1: nominal case: In this scenario, Delta robot is controlled to follow the reference trajectory at acceleration of 2.5 G, at speed of 1500 mm/s, and without any additional payload. The end-effector traverses the proposed trajectory for 10 cycles of the pick-and-place motion shown in Fig. 8.

The evolution of the Cartesian tracking errors of both implemented controllers is depicted in Fig. 15. It is worth to note, from this figure, the reduced dynamic errors by the proposed FF-ST-SMC algorithm, compared to the standard PIDFF control. The produced peak errors by the standard PIDFF control can be noticed larger than those of the proposed FF-ST-SMC, overall the whole trajectory and in the three axes.

The evaluation of the RMSEs show an improvement of 26 % and 31 % in terms of Cartesian and joint tracking errors, respectively (see Table VII). Better performance is verified by the proposed controller in terms of precision during dynamic motions.

The generated control signals by both controllers are illustrated in Fig. 16. The proposed FF-ST-SMC delivers control inputs of less amplitudes than those delivered by the standard PIDFF. This remarkable observation is quantified using the proposed input-torque-based criterion (54), giving an improvement of 19.5 % in terms of energy consumption (see Table VII).

2) Scenario 2: robustness towards payload and speed changes: This scenario imposes on the robot a high operating acceleration of 20 G and a speed of 2150 mm/s, while attaching to its end-effector a payload of mass 210 g. For safety purposes, the performed number of cycles is reduced to two cycles. The idea behind this scenario is to test the performance of the proposed control solution at high dynamic operating conditions (i.e. high acceleration and added payload).

The generated Cartesian tracking errors of both PIDFF and FF-ST-SMC controllers are sketched in Fig. 17. The proposed control solution gives better tracking performance, compared to the standard PIDFF at high-speed motions with an attached payload to the end-effector. Furthermore, less oscillations can be noticed in the Cartesian tracking errors coming from the proposed FF-ST-SMC, in comparison to those from the standard PIDFF.

The obtained RMSEs values are summarized in Table VIII. For Cartesian tracking errors, a reduction of 58 % from the standard PIDFF to the FF-ST-SMC algorithm is remarked, while a reduction of 53.5 % is remarked for joint tracking errors. Thanks to the robust terms of the proposed FF-ST-SMC, more disturbance-rejection is achieved, compared to the standard PIDFF. Thus, the robustness towards payload and speed changes of the proposed control approach is validated.

Figure 18 displays the evolution of the control signals provided by both controllers overall the reference trajectory. All the control signals are within the admissible range of

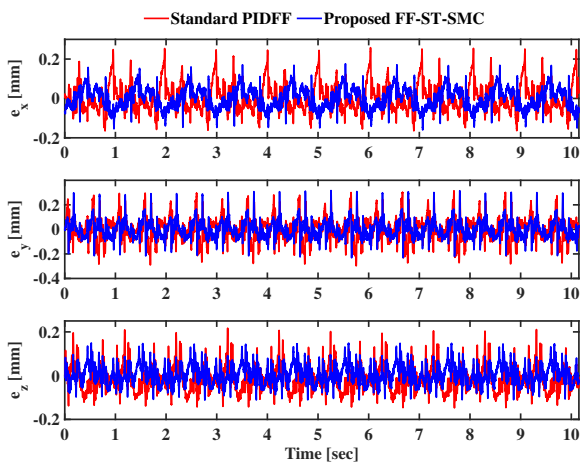

Fig. 15. Scenario 1: Evolution of the Cartesian tracking errors of both controllers used on Delta parallel robot.

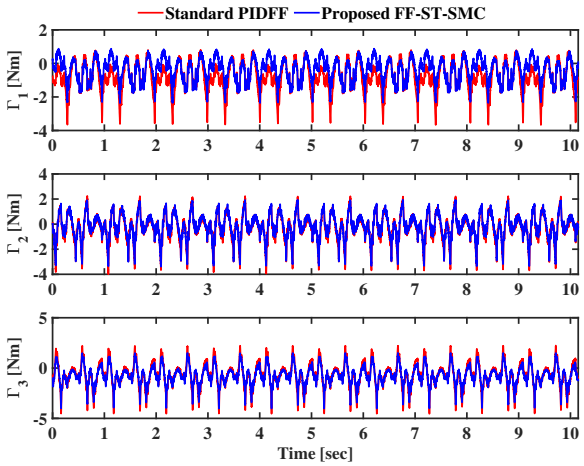

Fig. 16. Scenario 1: Evolution of the control input torques of both controllers used on Delta parallel robot.

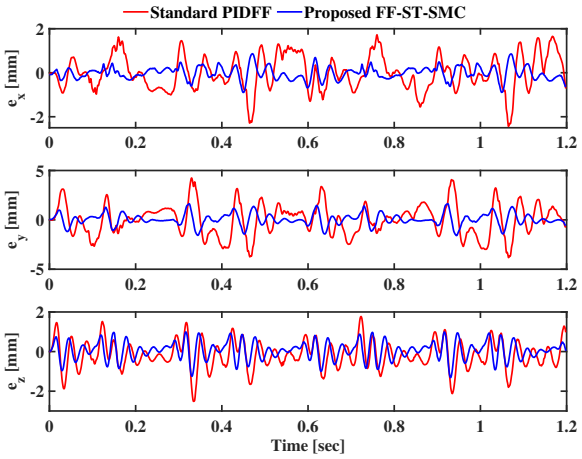

Fig. 17. Scenario 2: Evolution of the Cartesian tracking errors of both controllers used on Delta parallel robot.

the motors. However, smaller peak torques are produced by the proposed controller, compared to the PIDFF one. This reduction in energy consumption, from PIDFF to FF-ST-SMC controller, is evaluated to 22.1 %, as shown in Table VIII. In this scenario, the robot is performing pick-and-place motion cycles with increased acceleration and payload. Following the tracking trajectory, the robot encounters time-varying disturbances such as changes in the effects of inertia. This can be noticed by the change in the robot's acceleration. At the picking position, the robot starts from zero acceleration. Its acceleration goes up to a maximum value through the semi-elliptic motion. Then, the robot decelerates to zero while reaching the placing position. The time-varying change in acceleration can lead to a time-varying change in the effect of inertia. Thus, we can talk in this scenario about time-varying disturbances. However, the proposed controller is still more performant than a standard PIDFF controller, in terms of tracking precision and time-varying disturbance rejection.

3) Scenario 3: robustness towards very high accelerations: For a more challenging task, the Delta robot is configured to operate at a very high acceleration of 30 G and a speed of

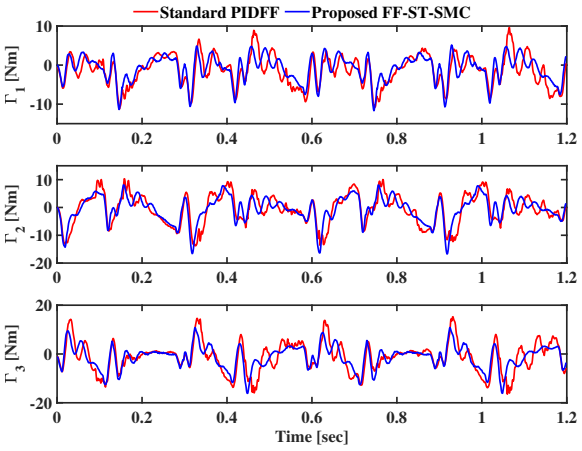

Fig. 18. Scenario 2: Evolution of the control input torques of both controllers used on Delta parallel robot.

TABLE VIII
SCENARIO 2: CONTROL PERFORMANCE EVALUATION OF BOTH CONTROLLERS USED ON DELTA PARALLEL ROBOT.

	$RMSE_T$ [mm]	$RMSE_J$ [deg]	E_Γ [Nm]
Standard PIDFF	1.9177	0.4355	1.5025×10^4
Proposed FF-ST-SMC	0.8064	0.2024	1.1706×10^4
Improvements	58 %	53.5%	22.1 %

2650 mm/s in this scenario. The pick-and-place trajectory of Fig. 8 is followed without any additional payload, for two motion cycles.

The evolution of the Cartesian tracking errors of both controllers is depicted in Fig. 19. Smaller dynamic errors and fewer oscillations are obtained for the proposed FF-ST-SMC algorithm, compared to the standard PIDFF. The Cartesian tracking trajectories of the PIDFF and FF-ST-SMC controllers are illustrated in 3D views in Figs. 21 and 22, respectively. One can observe better tracking accuracy for the proposed FF-ST-SMC algorithm, compared to the standard PIDFF controller.

The performance indices of both controllers for this scenario are summarized in Table IX. Improvements of 25 % and 28.9 % are noticed in the Cartesian and joint tracking errors for the proposed FF-ST-SMC over the standard PIDFF, respectively. The good dynamic performance and robustness of the proposed control approach at extremely high-speed motions are verified.

The control signals generated by both controllers, along the reference trajectory, are depicted in Fig. 20. Both the standard PIDFF controller and the proposed one deliver control input torques within the admissible ranges of the motors. However, the control signal of the FF-ST-SMC algorithm features smaller amplitudes than those of the PIDFF control. The improvement in terms of energy consumption by the proposed controller is quantified by 15.2 % as summarized in Table IX.

4) Accuracy versus operating acceleration: In this section, the RMSEs in Cartesian and joint spaces are computed for different operating accelerations of Delta robot, starting from 2.5 G up to 30 G. Two different cases are studied: with and without additional payload of mass 210 g.

The bar graph, depicted in Fig. 23, shows the variation of Cartesian and joint RMSEs in case of no added payload. The proposed controller generates better tracking errors at Cartesian and joint spaces, even with increased dynamic acceleration of Delta parallel robot. Thus, more robustness towards speed changes is validated by the proposed controller, compared to the standard PIDFF. Figure 24 depcites the variation of the RMSEs in case of added payload of mass 210 g. Better global dynamic performance of the proposed controller can be observed through the charts of RMSEs. The proposed controller overcomes the standard PIDFF in terms of parameters variation and speed changes.

To this end, the real-time experiments conducted on SPIDER4 and Delta robots demonstrate better dynamic performances provided by the proposed feedforward ST-SMC, compared to the standard feedforward PID control. To sum

up, superiority of the proposed controller has been validated in terms of precision, robustness towards operating condition changes, nonlinearities compensation, and disturbance-rejection.

5) Effect of the arms material: In all the aforementioned experimental results, the integrated rear arms of Delta parallel robot are made of Aluminum. In this section, we propose to replace the Aluminum rear arms with Carbon fiber ones, expecting better dynamic performances in terms of precision and robustness towards operating condition changes. Comparing the two arm types in terms of dynamic parameters, one can notice that both arms have approximately the same inertia ($0.0015\ Kg.m^2$) and close masses (0.0653 Kg for Aluminum arm and 0.062 Kg for Carbon fiber arm).

However, Carbon fibers are known by their extremely high modulus of elasticity and high strength. Carbon fiber can improve the strength of the driver arm while reducing its weight. Moreover, using Carbon fiber for designing the driver arms can also improve the strength-to-weight and stiffness-to-weight ratios of the whole robot structure.

To illustrate the significance of using Carbon fiber arms in industrial pick-and-place Delta parallel robot, the standard PIDFF controller and the proposed FF-ST-SMC algorithm are tested on Delta robot after integrating three Carbon fiber rear arms. A performance comparison is done between Aluminum and Carbon fiber arms at two main operating accelerations, also namely 2.5 G and 30 G, without any additional payload. Figure 25 shows the variation of the RMSE in Cartesian space with respect to arm material type and operating acceleration. One can see clearly that using Carbon fiber arms improves the global dynamic performance at low and high accelerations with both controllers. This improvement is summarized in Table X, showing a significant reduction of the $RMSE_T$ when using Carbon fiber arms (47.2 % with PIDFF control and 49.8 % with the proposed FF-ST-SMC algorithm). However, a small improvement is obtained from using Carbon fiber arms at low operating accelerations as shown in Table X.

To sum up, the effectiveness of Carbon fiber arms at high operating accelerations in compensating for the increasing nonlinearities of PKMs is validated through this experimental test.

VII. Conclusions and Future Work

In this work, a new feedforward ST-SMC approach is proposed as a control solution for robotic manipulators. The feedforward ST-SMC is composed of three main parts, including (i) a feedforward dynamic term, (ii) a feedback stabilizing term, and (iii) the standard ST-SMC term. The stability analysis of the proposed controller proves a local asymptotic convergence in a finite time. The proposed control

TABLE IX
Scenario 3: Control performance evaluation of both controllers used on Delta parallel robot.

	$RMSE_T$ [mm]	$RMSE_J$ [deg]	E_Γ [Nm]
Standard PIDFF	1.0732	0.2916	1.1556×10^4
Proposed FF-ST-SMC	0.8058	0.2074	9.7987×10^3
Improvements	25 %	28.9%	15.2 %

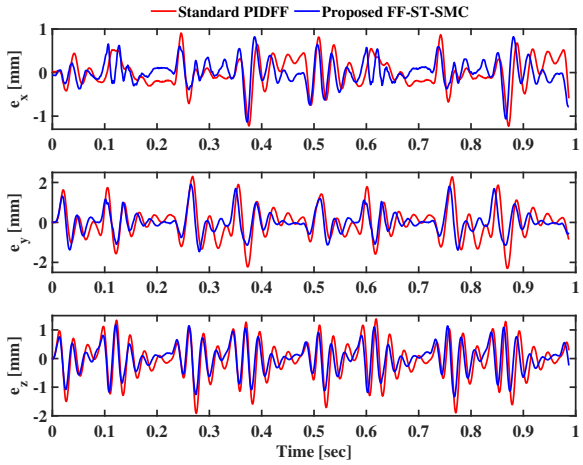

Fig. 19. Scenario 3: Evolution of the Cartesian tracking errors of both controllers used on Delta parallel robot.

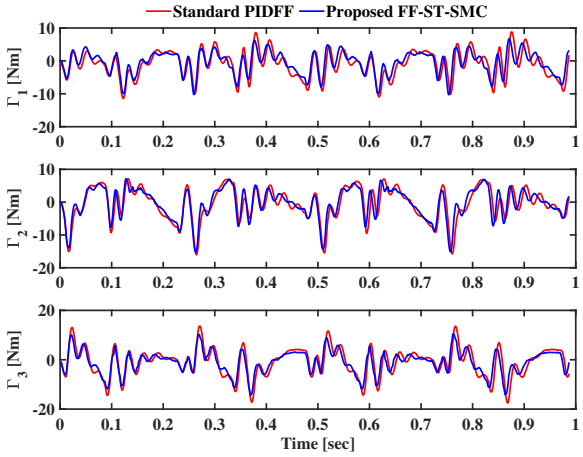

Fig. 20. Scenario 3: Evolution of the control input torques of both controllers used on Delta parallel robot.

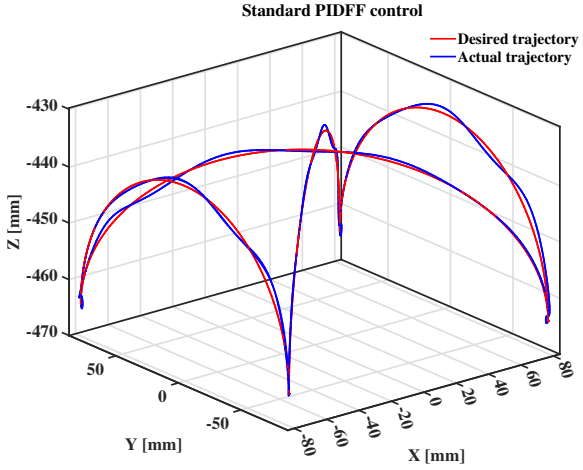

Fig. 21. Scenario 3: Evolution of the Cartesian tracking trajectories of the standard PIDFF control on Delta parallel robot.

TABLE X
$RMSE_T[mm]$ OF BOTH CONTROLLERS USED ON DELTA PARALLEL ROBOT WITH DIFFERENT ARM MATERIAL TYPES AND OPERATING ACCELERATIONS.

	2.5 G		30 G	
	PIDFF	FF-ST-SMC	PIDFF	FF-ST-SMC
Aluminum arms	0.1392	0.1031	1.0732	0.8058
Carbon fiber arms	0.126	0.1001	0.5667	0.4047
Improvements	9.5 %	3 %	47.2 %	49.8 %

solution was validated on two parallel kinematic manipulators in real-time framework. The obtained experimental results have shown better accuracy and robustness towards operating condition changes of the proposed controller, compared to other controllers from the literature.

As a future work, one can validate the proposed controller on a scenario of machining with SPIDER4 PKM, taking into account the relating issues (contact forces, compliance errors, stiffness, etc). Moreover, one can explore the design of an online dynamic adaptation mechanism for the proposed controller, taking into account the time-varying parameters (such as payload changes). In other words, design an adaptive controller that estimates the dynamic parameters of the model, especially the time-varying ones, with respect to system states (tracking error) changes. This may increase the robustness of the closed-loop system towards operating condition changes, and thus obtaining better dynamic performances.

REFERENCES

[1] Y. Shtessel, C. Edwards, L. Fridman, and A. Levant, *Sliding Mode Control and Observation*, ser. Control Engineering. New York, NY: Springer New York, 2014.

[2] M. Salim Qureshi, S. Das, P. Swarnkar, and S. Gupta, "Design And Implementation Of Sliding Mode Control For Uncertain Systems," *Materials Today: Proceedings*, vol. 5, no. 2, pp. 4299–4308, 2018.

[3] A. Bartoszewicz, "Discrete-time quasi-sliding-mode control strategies," *IEEE Transactions on Industrial Electronics*, vol. 45, no. 4, pp. 633–637, Aug. 1998.

[4] P.-M. Lee, S.-W. Hong, Y.-K. Lim, C.-M. Lee, B.-H. Jeon, and J.-W. Park, "Discrete-time quasi-sliding mode control of an autonomous underwater vehicle," *IEEE Journal of Oceanic Engineering*, vol. 24,

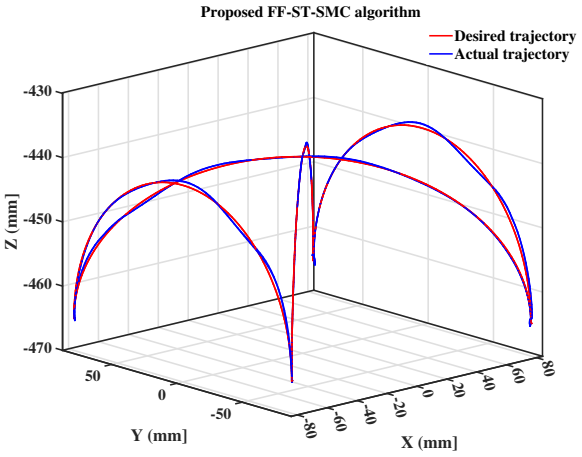

Fig. 22. Scenario 3: Evolution of the Cartesian tracking trajectories of the proposed FF-ST-SMC algorithm on Delta parallel robot.

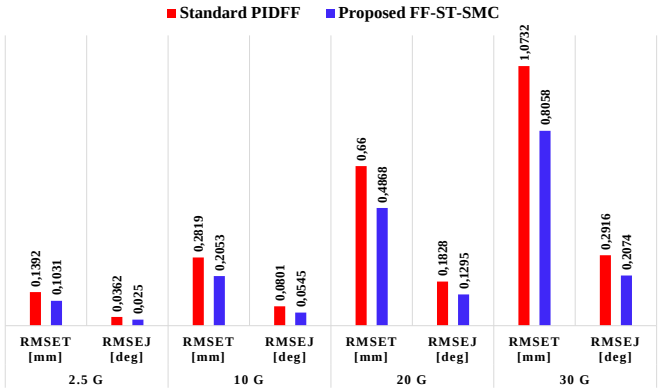

Fig. 23. Clustered column chart of RMSEs versus operating acceleration of Delta parallel robot with no payload.

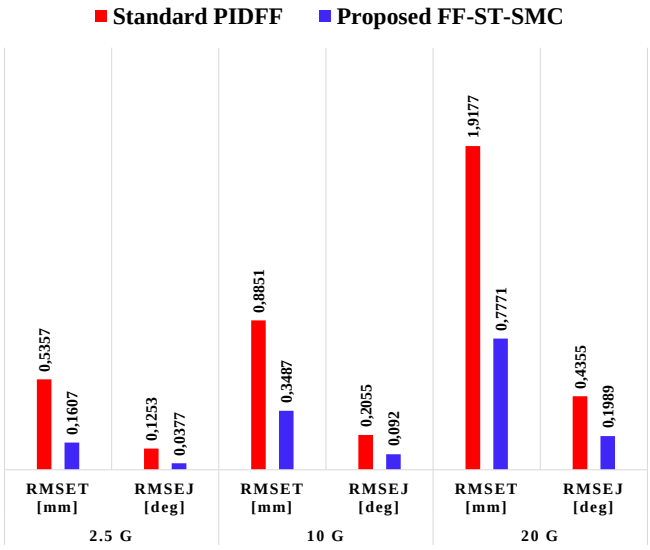

Fig. 24. Clustered column chart of RMSEs versus operating acceleration of Delta parallel robot with additional payload of 210 g.

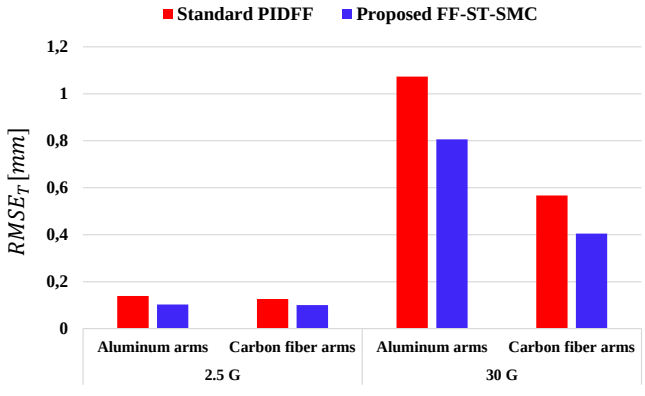

Fig. 25. Clustered column chart of $RMSE_T$ versus operating acceleration and arm material type of Delta parallel robot with no payload.

no. 3, pp. 388–395, Jul. 1999.

[5] E. Christopher and S. Spurgeon, *Sliding Mode Control: Theory And Applications*. CRC Press, 1998.

[6] M. Zhihong, A. Paplinski, and H. Wu, "A robust MIMO terminal sliding mode control scheme for rigid robotic manipulators," *IEEE Transactions on Automatic Control*, vol. 39, no. 12, pp. 2464–2469, Dec. 1994.

[7] S. V. Emel'yanov, S. K. Korovin, and A. Levant, "High-order sliding modes in control systems," *Computational Mathematics and Modeling*, vol. 7, no. 3, pp. 294–318, 1996.

[8] X. Yu and Z. Man, "Model reference adaptive control systems with terminal sliding modes," *International Journal of Control*, vol. 64, no. 6, pp. 1165–1176, Aug. 1996.

[9] A. Levant, "Sliding order and sliding accuracy in sliding mode control," *International Journal of Control*, vol. 58, no. 6, pp. 1247–1263, Dec. 1993.

[10] J. Rivera, L. Garcia, C. Mora, J. Juan, and S. Orteg, "Super-Twisting Sliding Mode in Motion Control Systems," in *Sliding Mode Control*, A. Bartoszewicz, Ed. InTech, Apr. 2011.

[11] L. Derafa, A. Benallegue, and L. Fridman, "Super twisting control algorithm for the attitude tracking of a four rotors UAV," *Journal of the Franklin Institute*, vol. 349, no. 2, pp. 685–699, Mar. 2012.

[12] R. Solea and D. Cernega, "Super twisting sliding mode controller applied to a nonholonomic mobile robot," in *2015 19th International Conference on System Theory, Control and Computing (ICSTCC)*. Cheile Gradistei, Romania: IEEE, Oct. 2015, pp. 87–92.

[13] S. Mobayen, F. Tchier, and L. Ragoub, "Design of an adaptive tracker for n-link rigid robotic manipulators based on super-twisting global nonlinear sliding mode control," *International Journal of Systems Science*, vol. 48, no. 9, pp. 1990–2002, Jul. 2017.

[14] T. Gonzalez, J. A. Moreno, and L. Fridman, "Variable Gain Super-Twisting Sliding Mode Control," *IEEE Transactions on Automatic Control*, vol. 57, no. 8, pp. 2100–2105, Aug. 2012.

[15] T. R. Oliveira, V. H. Pereira Rodrigues, A. Estrada, and L. Fridman, "Output-feedback variable gain super-twisting algorithm for arbitrary relative degree systems," *International Journal of Control*, vol. 91, no. 9, pp. 2043–2059, Sep. 2018.

[16] Y. Zhao, P. Huang, and F. Zhang, "Dynamic modeling and Super-Twisting Sliding Mode Control for Tethered Space Robot," *Acta Astronautica*, vol. 143, pp. 310–321, Feb. 2018.

[17] G. Sartori Natal, A. Chemori, and F. Pierrot, "Dual-space adaptive control of a redundantly actuated parallel manipulators for extremely fast operations with load changes," in *Proc. IEEE Int. Conf. on Robotics and Automat.*, St Paul, MN - USA,, 2012.

[18] M. Bennehar, A. Chemori, and F. Pierrot, "A new extension of direct compensation adaptive control and its real-time application to redundantly actuated pkms," in *Proc. IEEE/RSJ Int. Conf. Intel. Robots and Systems.*, Chicago, Il - USA, 2014.

[19] G. Sartori Natal, A. Chemori, and F. Pierrot, "Dual-Space Control of Extremely Fast Parallel Manipulators: Payload Changes and the 100g Experiment," *IEEE Transactions on Control Systems Technology*, vol. 23, no. 4, pp. 1520–1535, Jul. 2015.

[20] J.-P. Merlet, *Parallel robots*, 2nd ed., ser. Solid mechanics and its applications. Dordrecht ; Boston, MA: Kluwer Academic Publishers, 2006, no. 74.

[21] H. Cheng, Y.-K. Yiu, and Z. Li, "Dynamics and control of redundantly actuated parallel manipulators," *IEEE/ASME Transactions on Mechatronics*, vol. 8, no. 4, pp. 483–491, Dec. 2003.

[22] J. G. Ziegler and N. B. Nichols, "Optimum Settings for Automatic Controllers," *Journal of Dynamic Systems, Measurement, and Control*, vol. 115, no. 2B, pp. 220–222, Jun. 1993.

[23] H. Jingqing, "Nonlinear PID Controller," *Acta Automatica Sinica*, vol. 20, no. 04, pp. 487–490, Apr. 1994.

[24] H. Saied, A. Chemori, M. Bouri, M. El Rafei, C. Francis, and F. Pierrot, "A new time-varying feedback RISE control for second-order nonlinear MIMO systems: theory and experiments," *International Journal of Control*, vol. 0, pp. 1–14, Dec. 2019.

[25] H. Saied, A. Chemori, M. El Rafei, C. Francis, and F. Pierret, "Actuator and Friction Dynamics Formulation in Control of PKMs: From Design to Real-Time Experiments," in *2018 IEEE/RSJ International Conference on Intelligent Robots and Systems (IROS)*, Oct. 2018, pp. 5634–5639.

[26] H. Saied, A. Chemori, M. Michelin, M. El Rafei, C. Francis, and F. Pierrot, "A Redundant Parallel Robotic Machining Tool: Design, Control and Real-Time Experiments," in *New Developments and Advances in Robot Control*, ser. Studies in Systems, Decision and Control, N. Derbel, J. Ghommam, and Q. Zhu, Eds. Singapore: Springer, 2019, pp. 39–79.

[27] G. Sartori-Natal, A. Chemori, and F. Pierrot, "Nonlinear control of parallel manipulators for very high accelerations without velocity measurement: Stability analysis and experiments on par2 parallel manipulator," *Robotica*, vol. 34, no. 1, pp. 43–70, 2016, dOI: 10.1017/S0263574714001246.

[28] M. Bennehar, A. Chemori, and F. Pierrot, "A new revised desired compensation adaptive control for enhanced tracking: application to RA-PKMs," *Advanced Robotics*, vol. 30, no. 17-18, pp. 1199–1214, Sep. 2016.

[29] C. Huang, C. Chang, M. Yu, and L. Fu, "Sliding-mode tracking control of the Stewart platform," in *2004 5th Asian Control Conference (IEEE Cat. No.04EX904)*, vol. 1, Jul. 2004, pp. 562–569 Vol.1.

[30] P. Begon, F. Pierrot, and P. Dauchez, "Fuzzy sliding mode control of a fast parallel robot," in *Proceedings of 1995 IEEE International Conference on Robotics and Automation*, vol. 1. Nagoya, Japan: IEEE, 1995, pp. 1178–1183.

[31] R. Kumar, A. Chalanga, and B. Bandyopadhyay, "Smooth integral sliding mode controller for the position control of Stewart platform," *ISA Transactions*, vol. 58, pp. 543–551, Sep. 2015.

[32] H. B. Guo, Y. G. Liu, G. R. Liu, and H. R. Li, "Cascade control of a hydraulically driven 6-DOF parallel robot manipulator based on a sliding mode," *Control Engineering Practice*, vol. 16, no. 9, pp. 1055–1068, Sep. 2008.

[33] N.-I. Kim and C.-W. Lee, "High speed tracking control of Stewart platform manipulator via enhanced sliding mode control," in *Proceedings. 1998 IEEE International Conference on Robotics and Automation (Cat. No.98CH36146)*, vol. 3. Leuven, Belgium: IEEE, 1998, pp. 2716–2721.

[34] N.-I. Kim, C.-W. Lee, and P.-H. Chang, "Sliding mode control with perturbation estimation: application to motion control of parallel manipulator," vol. 6, no. 11, Nov. 1998, pp. 1321–1330.

[35] Y. Singh and M. Santhakumar, "Inverse dynamics and robust sliding mode control of a planar parallel (2-PRP and 1-PPR) robot augmented with a nonlinear disturbance observer," *Mechanism and Machine Theory*, vol. 92, pp. 29–50, Oct. 2015.

[36] M. Bennehar, G. El-Ghazaly, A. Chemori, and F. Pierrot, "A novel adaptive terminal sliding mode control for parallel manipulators: Design and real-time experiments," in *2017 IEEE International Conference on Robotics and Automation (ICRA)*. Singapore, Singapore: IEEE, May 2017, pp. 6086–6092.

[37] Z. Qi, J. E. McInroy, and F. Jafari, "Trajectory Tracking with Parallel Robots Using Low Chattering, Fuzzy Sliding Mode Controller," *Journal of Intelligent and Robotic Systems*, vol. 48, no. 3, pp. 333–356, Feb. 2007.

[38] J. Xu, Q. Wang, and Q. Lin, "Parallel robot with fuzzy neural network sliding mode control," *Advances in Mechanical Engineering*, vol. 10, no. 10, p. 168781401880126, Oct. 2018.

[39] H. Saied, A. Chemori, M. El Rafei, and C. Francis, "A Novel Model-Based Robust Super-Twisting Sliding Mode Control of PKMs: Design and Real-Time Experiments," in *2021 IEEE/RSJ International Conference on Intelligent Robots and Systems (IROS)*, Sep. 2021, pp. 8029–8035.

[40] J. A. Moreno and M. Osorio, "A Lyapunov approach to second-order sliding mode controllers and observers," in *2008 47th IEEE Conference on Decision and Control*. Cancun, Mexico: IEEE, 2008, pp. 2856–2861.

[41] B. Siciliano and O. Khatib, *Springer handbook of robotics*. Switzerland: Springer, Cham, 2016.

[42] C.-S. Jeong, J.-S. Kim, and S.-I. Han, "Tracking Error Constrained Super-twisting Sliding Mode Control for Robotic Systems," *International Journal of Control, Automation and Systems*, vol. 16, no. 2, pp. 804–814, Apr. 2018.

[43] F. L. Lewis, C. T. Abdallah, D. M. Dawson, and F. L. Lewis, *Robot manipulator control: theory and practice*, 2nd ed., ser. Control engineering series. New York: Marcel Dekker, 2004.

[44] R. Kelly, V. Santibáñez, and A. Loria, *Control of robot manipulators in joint space*, ser. Advanced textbooks in control and signal processing. London: Springer, 2005, oCLC: ocm58830429.

[45] H. K. Khalil, *Nonlinear Systems*. Prentice Hall, 2002, google-Books-ID: v_BjPQAACAAJ.

[46] J. M. Escorcia-Hernndez, A. Chemori, and H. Aguilar-Sierra, "Adaptive RISE Feedback Control for Robotized Machining With PKMs: Design and Real-Time Experiments," *IEEE Transactions on Control Systems Technology*, vol. 31, no. 1, pp. 39–54, 2023.

[47] J. M. Escorcia-Hernandez, A. Chemori, H. Aguilar-Sierra, and J. A. Monroy-Anieva, "A new solution for machining with ra-pkms: Modelling, control and experiments," *Mechanism and Machine Theory*, vol. 150, p. 103864, 2020.

[48] R. Clavel, "Device for the movement and positioning of an element in space," US Patent US4 976 582A, Dec., 1990.
[49] M. Bennehar, A. Chemori, M. Bouri, L. Jenni, and F. Pierrot, "A new RISE-based adaptive control of PKMs: design, stability analysis and experiments," *International Journal of Control*, vol. 91, no. 3, pp. 593–607, Mar. 2018.
[50] A. Codourey, "Dynamic Modeling of Parallel Robots for Computed-Torque Control Implementation," *The International Journal of Robotics Research*, vol. 17, no. 12, pp. 1325–1336, Dec. 1998.
[51] A. Mueller, "Effects of geometric imperfections to the control of redundantly actuated parallel manipulators," in *2009 IEEE International Conference on Robotics and Automation*. Kobe: IEEE, May 2009, pp. 1782–1787.
[52] T. Hufnagel and A. Muller, "A Projection Method for the Elimination of Contradicting Decentralized Control Forces in Redundantly Actuated PKM," *IEEE Transactions on Robotics*, vol. 28, no. 3, pp. 723–728, Jun. 2012.

Hussein Saied received the Electrical Engineering degree from Lebanese University, Beirut, Lebanon, in 2016, the M.Sc. degree in automatic control from the Lebanese University, Beirut, Lebanon and University of Technology of Compiegne, Compiegne, France, in 2016, and the Ph.D. in automatic control from University of Montpellier and Lebanese University in 2019. He is currently a Postdoctoral Fellow with the Engineering School SIGMA-Clermont, Clermont-Ferrand, France. His research interests include automatic control and robotic manipulators.

Ahmed Chemori received the M.Sc. and Ph.D. degrees both in automatic control from the Grenoble Institute of Technology, Grenoble, France, in 2001 and 2005, respectively. He has been a Postdoctoral Fellow with the Automatic Control Laboratory, Grenoble, France, in 2006. He is currently a tenured Research Scientist in automatic control and robotics with the Montpellier Laboratory of Informatics, Robotics, and Microelectronics. His research interests include nonlinear, adaptive, and predictive control and their applications in robotics.

Mohamed Bouri obtained his PhD thesis in 1997 from INSA-Lyon (Fr). As a roboticist, he is specialized in the development and control of robotic structures and is active in the design of fast and high precision robots for industrial applications. He leads the research group Rehabilitation and Assistive Robotics (REHAssist) at Ecole Polytechnique Fdrale de Lausanne (EPFL). His current research focuses on Medical robotics for rehabilitation, lower limb exoskeletons and surgical applications.

Maher El Rafei received his M. Eng. degree in Industrial Control from the Lebanese University (2004). He received his M.Sc. and Ph.D. degrees, both in Automatic Control from The University of Montpellier II (2005) and Grenoble Institute of Technology (2008), France. He is currently an associate professor at the Lebanese University and a researcher in Automatic Control and Robotics at CRSI. His research interests include nonlinear control with special emphasis on their real-time applications in robotics.

Clovis Francis received his Engineering degree from the Lebanese University, Faculty of Engineering in 1990, the Master degree from the University Paul SabatierToulouse in 1991, the Ph.D. degree from the University paris XI France in 1994 and the Accredidation to Supervise Research (HDR) in 2009. Currently he is a Professor at the Lebanese University in Automatic Control, Fault Tolerant Control and system diagnosis.